A&A 529, A44 (2011)
DOI: 10.1051/0004-6361/201014105

Astronomy & Astrophysics

Dust in brown dwarfs and extra-solar planets

III. Testing synthetic spectra on observations

S. Witte[1], Ch. Helling[2], T. Barman[3], N. Heidrich[1], and P. H. Hauschildt[1]

[1] Hamburger Sternwarte, Gojenbergsweg 112, 21029 Hamburg, Germany
e-mail: switte@hs.uni-hamburg.de
[2] SUPA, School of Physics and Astronomy, University of St. Andrews, North Haugh, St. Andrews KY16 9SS, UK
[3] Lowell Observatory, 1400 West Mars Hill Road, Flagstaff, AZ 86001, USA

Received 20 January 2010 / Accepted 18 January 2011

ABSTRACT

Context. This work is concerned with dust formation in ultra-cool atmospheres, encompassing the latest type stars, brown dwarfs, and hot giant exoplanets. Dust represents one of the most important and yet least understood sources of opacity in these types of objects.
Aims. We compare our model spectra with SpeX data in order to draw conclusions about the dust cloud structure and related quantities in ultra-cool atmospheres.
Methods. We use the self-consistent Drift-Phoenix atmosphere code, which features a kinetic dust formation mechanism and accounts for the dust cloud influence on the spectra.
Results. We present fits of our latest model spectra to observations that cover a wide range of our model grid. The results are remarkably good, yielding significant improvement over the older Cond-/Dusty-Phoenix models, especially in the L-dwarf regime. The new models are able to properly reproduce observed spectra, including complicated features such as the molecular band strengths. This raises confidence in the reliability of our dust-modeling approach.
Conclusions. We demonstrate that our code produces excellent results concerning the fitting with observations. This suggests that our dust cloud and atmosphere structures are reasonably accurate. Like all other current cloud models, ours is not able to produce satisfying results for spectral types later than L6 without manually tuning down the amount of dust. Our results show the formation of convective cells within the cloud, which are able to destroy the lower cloud parts. The dust opacity is reduced significantly without the need to tune the dust cloud thickness. There are indications that the cycle of dust accumulation and cloud destruction by convection is time-dependent on rather long timescales. Considering a statistical distribution of locally variable dust clouds over a dwarf's surface can result in a large number of spectral configurations for the same model atmosphere parameters, hence introducing an additional and more or less random degree of freedom to those atmospheres. Without resorting to the model atmosphere parameters, this alone can account for the unusually red and blue objects that have been discovered.

Key words. astrochemistry – methods: numerical – stars: atmospheres – stars: low-mass – brown dwarfs

1. Introduction

The complexity of stellar atmospheres increases considerably with decreasing effective temperature. Molecules start to form, thereby reducing the strength of atomic lines by consuming the respective elements and reducing the spectral contrast. On the other hand, molecules themselves represent strong absorbers and cause significant heating of the local gas (e.g., Allard et al. 1997). Making matters even more complicated, the influence of gas molecules begins to be outdone by the onset of condensation in the latest types of stars (Tsuji et al. 1996). Gas molecules begin to stick together, at first by polymerization and then also by surface reactions. Subject to the stellar gravity, the forming dust grains eventually fall inwards, taking a significant portion of the heavy elements of the upper atmosphere with them. Moreover, the forming dust clouds provide an enormous opacity (Jones & Tsuji 1997). As a result, the spectral appearance of the object is considerably changed, while the local gas at the cloud can by heated by up to several hundred Kelvins compared to a dust-free atmosphere (e.g., Witte et al. 2009). Another aspect of the problem is the element replenishment of the upper atmosphere, which is driven by the weak gas motion above the convection zone (Ludwig et al. 2002). It closes the cycle of dust formation and gravitational settling and keeps the mechanism running. The result is a mostly stationary dust cloud that encompasses the object (Woitke & Helling 2004). While dust clouds emerge in late M-dwarfs, the lowest mass stars, their influence magnifies enormously for the mid-L types, which represents brown dwarfs. Only for considerably later spectral types, where the dust clouds sink out of the visible parts of the atmosphere, its spectral impact does decrease.

Until the work of Hayashi (1962) and Kumar (1963), it was believed that objects of a few percent of a solar mass were not able to form at all. More recent simulations (Whitworth 2007) predict a "stellar formation" limit close to a Jupiter mass. The continuous nuclear burning of hydrogen requires a minimum of roughly 0.07 solar masses for solar element abundances (Chabrier & Baraffe 2000). Forming objects that exceed this value will become full-fledged stars by settling onto the main sequence, i.e., achieving an equilibrium between gravity and radiation-sustained gas pressure. In contrast, objects of less mass will not reach this stability, because no lasting hydrogen burning

is possible. Since they lack continuous nuclear burning as an energy source, these substellar objects or brown dwarfs are continuously contracting and cooling while radiating away gravitational energy (e.g., Chabrier et al. 2000). This means that the age has an enormous impact on the spectral appearance of the brown dwarf. For main sequence stars, unambiguous and well-constrained relations between stellar parameters like mass or effective temperature and the spectral type can be derived. This is no longer the case for brown dwarfs, where objects of comparable spectral type can differ strongly in age and mass. To account for these properties, the implied spectral diversification caused by the surface gravity and metallicity have to be considered when classifying observations (e.g., Kirkpatrick 2005).

The first L dwarf has been observed as early as 1987 (Becklin & Zuckerman 1988). Several years later, the first expressly declared brown dwarfs were reported (Rebolo et al. 1995), though their substellarity did not achieve global acceptance at the time. Shortly after, Nakajima et al. (1995) reported the discovery of Gl229B. Their analysis incontrovertibly characterized it as a brown dwarf.

In subsequent years, large numbers of brown dwarfs were identified, which can be attributed to surveys such as 2MASS (Kleinmann 1992).

The importance of dust in ultra-cool atmospheres has first been noted by Lunine et al. (1986). Shortly after the first confirmed discovery of a brown dwarf, observational evidence for dust (Noll et al. 1997) as well as first dust modeling results for brown dwarfs (Tsuji et al. 1996) were presented. Since then, several more groups have been developing models and studying the atmospheric dust formation in ultra-cool dwarfs (Burrows & Sharp 1999; Allard et al. 2001; Ackerman & Marley 2001; Cooper et al. 2003; Woitke & Helling 2003). A detailed comparison between the different modeling approaches has been published by Helling et al. (2008a). In order to reproduce observations, a proper dust treatment is mandatory for any atmosphere simulation of brown dwarfs. In the present paper, we present our latest modeling results with Drift-Phoenix (Witte et al. 2009) which benefitted from a much improved gas-phase chemistry and test them on observations.

2. Method

We use the Drift-Phoenix model atmosphere code (Dehn 2007; Helling et al. 2008b) in the most recent version presented by Witte et al. (2009). The general-purpose model atmosphere code Phoenix (Hauschildt & Baron 1999; Baron et al. 2003) solves the gas-phase equation of state, provides the atmosphere structure to Drift, determines the gas opacities and solves the radiative transfer. On the other hand, the Drift code by Helling et al. (2008c) returns a consistent dust cloud structure with corresponding opacities and the altitude-dependent depletion and redistribution of gas phase abundances, which feed back on both the thermodynamical structures and the radiation field. An iteration of this method allows the determination of stationary atmosphere and dust cloud properties and yields the respective synthetic spectra.

In Drift, the dust formation is considered to proceed via the formation of seed particles and their subsequent growth or evaporation. We solve a system of dust moment and element conservation equations that take into account the nucleation, growth and evaporation processes in the phase non-equilibrium and the influence of gravitational settling and element replenishment by convective overshooting on these dust formation processes. The modified classical nucleation theory of Gail et al. (1984) is applied to determine the nucleation rate (for more details see Woitke & Helling 2004). The dust growth of dirty particles is modeled according to Woitke & Helling (2003), Helling & Woitke (2006) and Helling et al. (2008c). Here, we consider only the seven most important solids (TiO_2[s], Al_2O_3[s], Fe[s], SiO_2[s], MgO[s], $MgSiO_3$[s], Mg_2SiO_4[s]) made of six different elements. The growth of the grains is governed by the supersaturation ratio of the gas and is triggered by the actual collision rates between grains and gas molecules and, therefore, depends on the grain surface. Thus, the model does not enforce a phase equilibrium. The local number and size of dust grains as well as their mean composition throughout the atmosphere are natural results of the model. We include mixing by convection and overshooting by assuming an exponential decrease in mass exchange frequency in the radiative zone (Woitke & Helling 2004). The opacities of the composite dust particles are calculated by using effective medium theory (Bruggeman 1935) and Mie theory (Mie 1908; Wolf & Voshchinnikov 2004). The grain size distribution is a native result of the dust model. Given the uncertainties of current models with respect to the dust opacity, a simple double delta-peaked function is assumed for the opacity calculation. Likewise, the considered grain composition corresponds to local mean values. Typical grain sizes for near-solar abundances range from several nanometers to several tenths of a micrometer.

The model code Drift-Phoenix has been discussed in more detail by Witte et al. (2009). Since then, the most significant improvement of the code has been the implementation of the EOS module ACES (Barman, in prep.).

3. Results

Previous tests of Drift-Phoenix on observations have been presented by Helling et al. (2008b), Schmidt et al. (2008), Neuhäuser et al. (2009), and Burgasser et al. (2009).

Witte et al. (2009) gave a more general analysis of dust and atmosphere properties over the parameter space. The current Drift-Phoenix model atmospheres grid covers the following model atmosphere parameters:

Parameter	Minimum	Maximum	Increment
$T_{\rm eff}$	1000 K	3000 K	100 K
$\log(g)$	3.0	5.5	0.5
[M/H]	−0.6	+0.3	0.3

For the present work, we used the corresponding synthetic spectra to fit dwarf spectra which we have acquired from `DwarfArchive.org`. After eliminating too early and too late spectral types as well as known binaries, peculiar and overly noisy observations, 108 observations remained. For those we have determined the model atmosphere parameters through fitting. The fits were carried out by a plain χ^2-minimization for a simple scaling factor in the range of 0.7...2.4 μm, with the goodness-of-fit definition of Burgasser et al. (2009) as criterion to identify the best fitting models. In ambiguous cases, the fits were checked by eye to obtain the best possible fit. To achieve a better fitting result, the synthetic high resolution spectra were degraded to the required resolution.

In this section, a discussion of 18 sample fits is given (Table 1). The corresponding fits are shown in Figs. 1 through 18. The discussed and shown objects were chosen to provide a wide impression for the model quality over the presently available parameter space of observations. The remaining 90 fits are included in the general discussion in the next section.

Table 1. Discussed sample objects.

token	Object designation	Observation optical SpT	NIR SpT	observation by	DRIFT-PHOENIX best fit $T_{\rm eff}$ [K]	log(g)	[M/H]	Figure
J0403	2MASS J04035944+1520502	–	M7	Burgasser et al. (2004)	3000	5.0	−0.0	1
J0011	2MASS J00115060-1523450	–	M7.5Ve	Burgasser et al. (2004)	2700	4.5	−0.0	2
J0033	2MASS J00335534-0908247	–	M8Ve	Burgasser et al. (2004)	2700	4.0	−0.0	3
J1139	2MASS J11395113-3159214	M8	M9pec	Looper et al. (2007)	2500	3.5	−0.3	4
LP944	LP944-20	M9	–	Burgasser et al. (2008a)	2000	5.5	+0.3	5
J0457	2MASS J04574903+3015195	M9.25	–	Muench et al. (2007)	2600	3.5	−0.0	6
J0141	2MASS J01415823-4633574	L0	L0pec	Kirkpatrick et al. (2006)	1700	4.0	−0.0	7
J1439	2MASS WJ1439284+192915	L1	–	Burgasser et al. (2004)	2100	5.0	+0.3	8
J2057	2MASS J2057540-025230	L1.5	L1.5	Burgasser et al. (2004)	1900	5.0	+0.3	9
J0921	2MASS J09211410-2104446	L2	L4	Burgasser et al. (2007)	2000	5.0	+0.3	10
J0241	2MASS J0241536-124106		L2	Burgasser et al. (2008a)	1800	5.0	−0.0	11
J1207	2MASS J12070374-3151298	L3		Siegler et al. (2007)	1700	5.0	−0.0	12
J1506	2MASS WJ1506544+132106	L3		Burgasser (2007)	1700	4.0	−0.0	13
J1507	2MASS WJ1507476-162738	L5	L5.5	Burgasser (2007)	1800	5.0	−0.0	14
J1010	2MASS J1010148-040649	L6	–	Reid et al. (2006)	1700	4.5	−0.0	15
J2148	2MASS J21481628+4003593	L6	L6.5pec	Looper et al. (2008)	1500	3.0	−0.3	16
J2244	2MASS J2244316+204343	L6.5	L7.5pec	Looper et al. (2008)	1500	3.5	+0.3	17
J2101	2MASS J2101154+175658	L7.5*	L6.5*	Chiu et al. (2006)	1600	4.5	+0.3	18

Notes. (*) Reported binary.

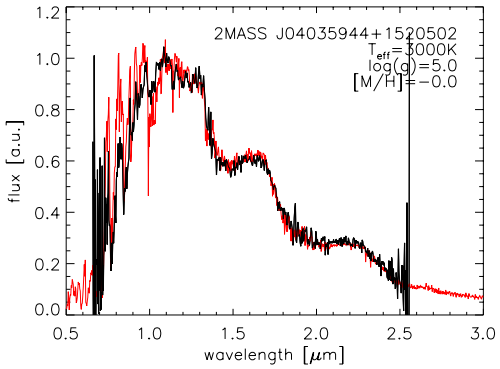

Fig. 1. 2MASS J04035944+1520502 (M7) (Burgasser et al. 2004): observation (black) and best fitting model (red).

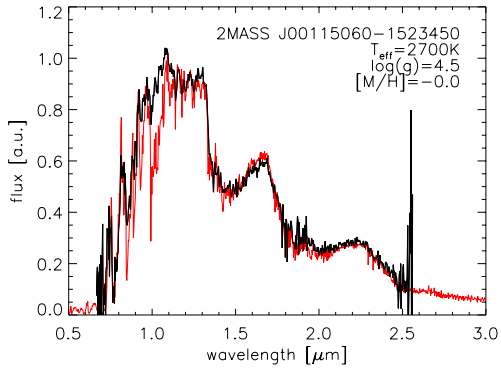

Fig. 2. 2MASS J00115060-1523450 (M7.5) (Burgasser et al. 2004): observation (black) and best fitting model (red).

J04035944+1520502 (M 7; Fig. 1, best fit: $T_{\rm eff}$ = 3000 K, $\log g$ = 5.0, [M/H] = 0.0): The dwarf J0403 is among the earliest spectral types which can be fit with the present model grid. Its spectral shape as well as finer features are rather well reproduced by the best fitting model. Of the following 18 objects, J0403 is the only one that does not contain dust in its atmosphere.

J00115060-1523450 (M 7; Fig. 2, best fit: $T_{\rm eff}$ = 2700 K, $\log g$ = 4.5, [M/H] = 0.0): The second object in our sample, J0011, is among the hottest objects featuring dust within the outer reaches of their atmosphere. According to our models, condensation sets in for effective temperatures slightly above 2800 K. The influence of the clouds can hardly be observed directly in objects like J0011, as the efficiency of the dust formation is still weak and the few grains yield only low opacities. In contrast, indirect effects may already become visible, as the gas phase amount of metals is already depleted due to the dust formation. Especially, the more rare elements such as, e.g., Al and Ti show depletion rates of up to 50% at the cloud. The undepleted and still visible high density layers below the cloud will render the resulting influence irrelevant in the spectrum of J0011. However, for lower effective temperatures the dust cloud turns optically thicker and starts to overshadow the layers below, while the gas phase depletion at the cloud becomes stronger. Therefore, the above described effect becomes significant for later M-type dwarfs and strongly contributes to the vanishing of the TiO and VO features, observed in the spectra of cooler objects. The observation of J0011 is very well matched by the model, except for the overestimated FeH band at about 1 μm. Though best fit indicates a log(g) of 4.5, the goodness of fits for the given wavelength range and resolution is not sensitive enough to exclude a higher and more likely gravity. For later spectral types, the influence of gravity becomes considerably more important and allows a more reliable determination with the employed fitting method.

J00335534-0908247 (M 8; Fig. 3, best fit: $T_{\rm eff}$ = 2700 K, $\log g$ = 4.0, [M/H] = 0.0): The object J0033 was designated to be of spectral type M8 (Burgasser et al. 2004), not very different from J0011. With respect to the effective temperatures, both objects appear to be comparable. However, J0033 appears to be a younger dwarf, according to our best fit surface gravity and the trend represented by the goodness of fit of surrounding models.

Compared to J0011, J0033 distinguishes itself by the weaker red optical part, weaker FeH features in the J band, the slightly

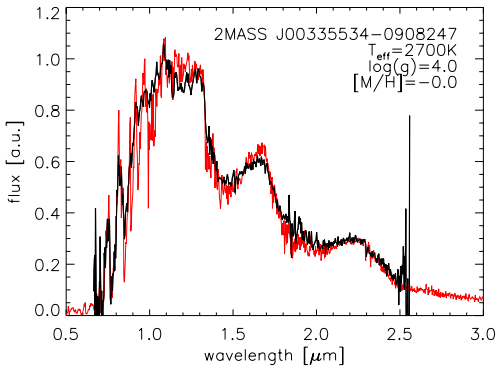

Fig. 3. 2MASS J00335534-0908247 (M8) (Burgasser et al. 2004): observation (black) and best fitting model (red).

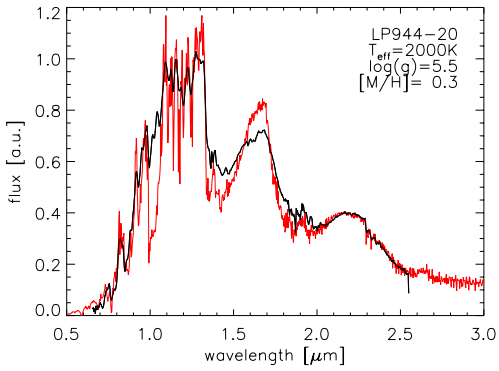

Fig. 5. LP944-20 (M9) (Burgasser et al. 2008a): observation (black) and best fitting model (red).

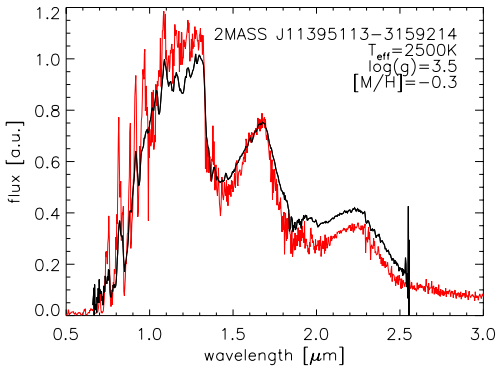

Fig. 4. 2MASS J11395113-3159214 (M9) (Looper et al. 2007): observation (black) and best fitting model (red).

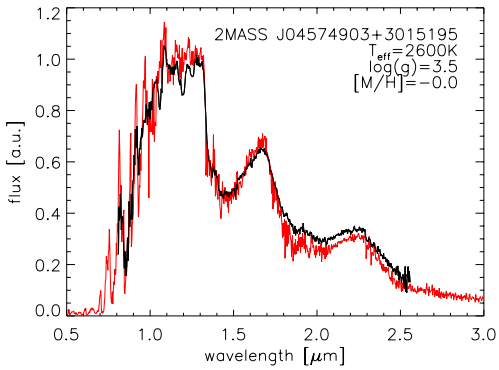

Fig. 6. J04574903+3015195 (M9.25) (Muench et al. 2007): observation (black) and best fitting model (red).

enhanced flux in H band, as well as slightly stronger H_2O and CO bands. Still, both spectra look fairly alike and are both very well matched by our synthetic spectra.

J11395113-3159214 (M 9pec; Fig. 4, best fit: $T_{\rm eff}$ = 2500 K, $\log g$ = 3.5, [M/H] = −0.3): According to our best fit parameters, J1139 is a young late M-type object which agrees with the conclusions by Looper et al. (2007). Its implied effective temperature suggests that its atmospheres already contains a considerable amount of dust and a noteworthy backwarming at the bottom of the cloud is affecting the emerging radiative field. The spectral contour of J1139 is more or less well matched. The water band strengths, the CO band head and the shape of the H and K bands are well matched. In contrast, the J band of the observation shows a slightly too high flux while the K band is underrepresented. Nonetheless, individual features seem to agree within both bands. Hence, the best fit model atmosphere parameters seem to be roughly appropriate, though a slightly lower effective temperature might turn out as beneficial with respect to the model colors. However, an improvement of the J and K band fluxes by variation of the model atmosphere parameters can only be achieved at the expense of the triangular shape of the H band and the water band strengths.

Rice et al. (2010) have recently published narrow band fits for J1139, using Dusty-Phoenix spectra. They have found a surface gravity comparable to ours. Both effective temperature estimates are in good agreement, differing by only about 100 K.

LP944-20 (M 9; Fig. 5, best fit: $T_{\rm eff}$ = 2000 K, $\log g$ = 5.5, [M/H] = +0.3): LP994-20 represents the first definite brown dwarf in our selection of objects. Tinney (1998) demonstrated the high Li abundance of LP994-20, substantiating the substellarity. Ribas (2003) estimated its effective temperature to be close to 2000 K and suggested near-solar abundances. Our estimate agrees in both respects. The model is very good at reproducing the red optical slope and the K band. Surprisingly, it overrates the water bands around 1.5 and 2.0 μm and overestimates the H band peak. A reduction of metallicity is not able to adjust them considerably and would worsen the well-matched K band. Our models properly reproduce the water bands of objects like J1139 (Fig. 5), which is of a similar spectral type as LP944-20. While the shown best fit of J1139 probably indicated a slightly too high effective temperature, the weaker water bands of LP944-20 suggest an underestimation of the effective temperature. This might be explained by a too weak reddening of the high gravity models with decreasing effective temperature above 2000 K.

J04574903+3015195 (M 9.25; Fig. 6, best fit: $T_{\rm eff}$ = 2600 K, $\log g$ = 3.5, [M/H] = 0.0): Being classified as a marginally later type than LP994-20, J0457 has been characterized as a young dwarf (Kraus & Hillenbrand 2009), just as J1139. In contrast to the former objects, the observation of J0457 is very well matched by the model. Its J band flux is notably stronger than that of J1139, which results in a higher best fit effective temperature and a considerably better agreement. Our best fit surface gravity is consistent with the conclusion of J0457's youth.

J01415823-4633574 (L0pec; Fig. 7, best fit: $T_{\rm eff}$ = 1700 K, $\log g$ = 4.0, [M/H] = 0.0): Kirkpatrick et al. (2006) identified

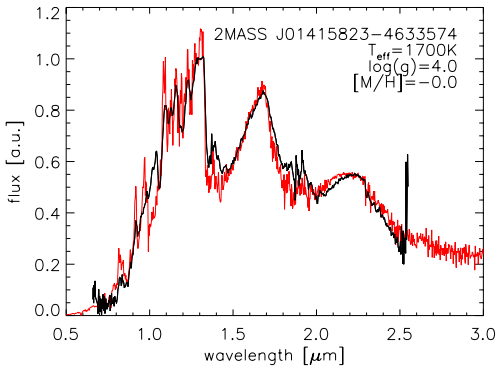

Fig. 7. 2MASS J01415823-4633574 (L0) (Kirkpatrick et al. 2006): observation (black) and best fitting model (red).

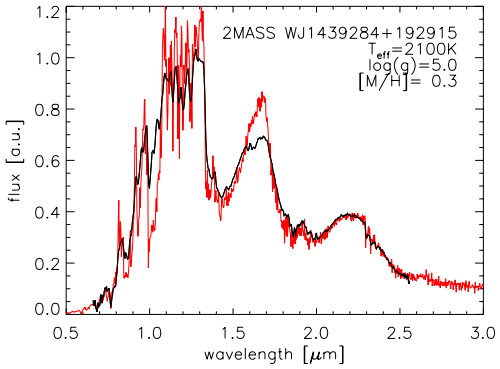

Fig. 8. 2MASS WJ1439284+192915 (L1) (Burgasser et al. 2004): observation (black) and best fitting model (red).

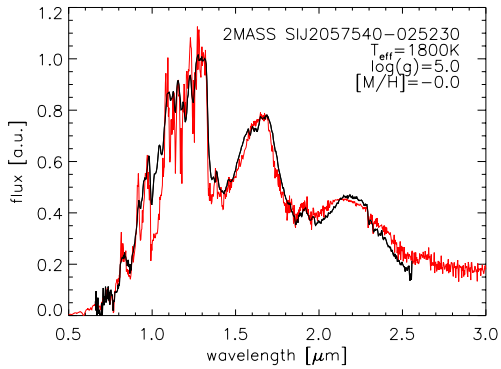

Fig. 9. 2MASS IJ2057540-025230 (L1.5) (Burgasser et al. 2004): observation (black) and best fitting model (red).

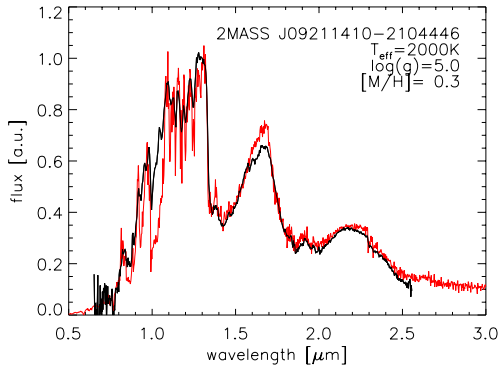

Fig. 10. 2MASS J09211410-2104446 (L2) (Burgasser et al. 2007): observation (black) and best fitting model (red).

J0141 as a young early-L dwarf, a conclusion which was confirmed by Reid et al. (2008). Empirically, Kirkpatrick et al. (2006) estimated model atmosphere parameters of $T_{\rm eff} \approx 2200$ K and a $\log(g)$ of 4.0. Their comparison with DUSTY-PHOENIX models yielded $T_{\rm eff} = 2000$ K and $\log(g) = 4.0$. The DRIFT-PHOENIX models are suited to take into account the water bands, which had to be neglected in the DUSTY-PHOENIX fit by Kirkpatrick et al. (2006). Surprisingly, the water band strength of the object leads to a much lower effective temperature estimate for J0141 with our models. The determined best fit is very unambiguous and appears to be reproducing the overall spectral shape, as well as the individual band shapes and molecular bands extraordinarily well. Our determined $\log(g) = 4.0$ is in good agreement with the empirical result of Kirkpatrick et al. (2006). Therefore, we can reinforce the estimated young age of J0141. On the other hand, our best fit effective temperature of 1700 K is considerably lower than their empirical value. Indeed, J0141 requires a model of very red NIR colors for a good fit. The necessary redness is only reached at about 1700 K for the employed model grid. As noted before (see LP944-20), the models appear to be reddening slightly too slow, which might have caused an underestimation of the effective temperature of J0141. Nevertheless, such a lower effective temperature apppears to have no considerable impact on the mass and age estimate made by Kirkpatrick et al. (2006, Fig. 10).

WJ1439284+192915 (L1; Fig. 8, best fit: $T_{\rm eff} = 2100$ K, $\log g = 5.0$, [M/H] = +0.3): J1439 is the first old L dwarf in our sample. The red optical slope and the K band are very well reproduced by the best fitting model. Unfortunately, the model is showing a too high flux in the J and H peaks, i.e., the model is again pointing at a too blue SED for its effective temperature.

J2057540-025230 (L1.5; Fig. 9, best fit: $T_{\rm eff} = 1900$ K, $\log g = 5.0$, [M/H] = +0.3): Compared to J1439, the object J2057 is notably redder and, therefore, of slightly later spectral type. Hence, our best fitting model (Fig. 9) points to a lower effective temperature. Between the red optical range and the CO band edge longwards of the K band, the model agrees quite well with the observation. Unfortunately, the best fit is considerably cooler than that of J1439. Hence, the effective temperature of J2057 might be underestimated by the fit.

J09211410-2104446 & J0241536-124106 (both L2; Figs. 10, 11, best fits: $T_{\rm eff} = 2000$ K, $\log g = 5.0$, $[M/H] = +0.3$ and $T_{\rm eff} = 1800$ K, $\log g = 5.0$, [M/H] = 0.0): J0921 and J0241 have both been characterized as L2 types by Burgasser et al. (2007) and Burgasser et al. (2008b), respectively. However, in the case of J0241 the flux in the H and K bands is significantly catching up with that of the J band and the strong water bands around 1.5 and 2.0 μm and the CO band beginning at 2.3 μm become stronger. In agreement with that, Reid et al. (2008) have found a spectral type of L1.5 for J0921. Our best fits agree with the distinction of the spectral types of both objects, as J0241 appears a little cooler. The spectral shape of both objects are well emulated and spectral features in the red optical and even within the water bands (1.5 and 2.0 μm) are nicely reproduced.

J12070374-3151298 (L3; Fig. 12, best fit: $T_{\rm eff} = 1700$ K, $\log g = 5.0$, [M/H] = 0.0): Looking somewhat alike to J0241

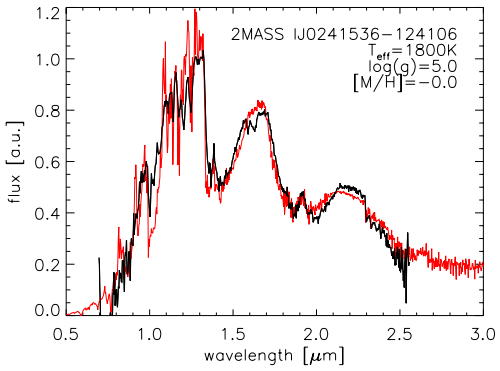

Fig. 11. 2MASS IJ0241536-124106 (L2) (Burgasser et al. 2008a): observation (black) and best fitting model (red).

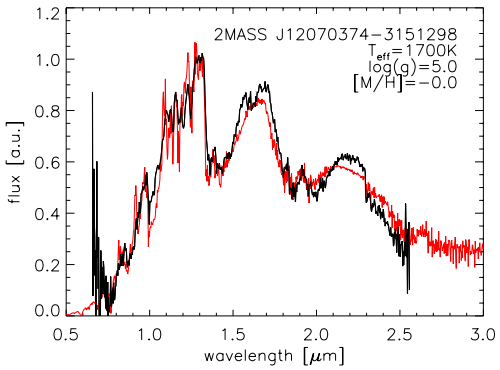

Fig. 12. 2MASS J12070374-3151298 (L3) (Siegler et al. 2007): observation (black) and best fitting model (red).

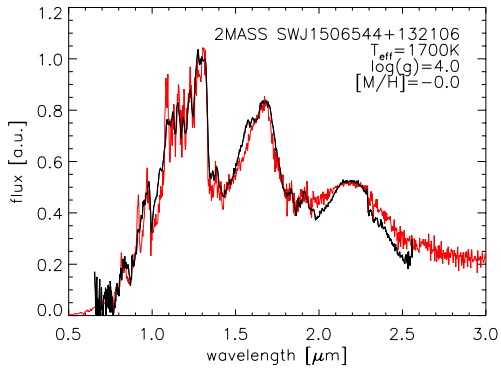

Fig. 13. 2MASS WJ1506544+132106 (L3) (Burgasser 2007): observation (black) and best fitting model (red).

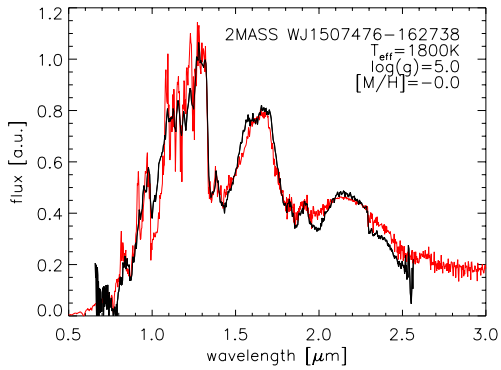

Fig. 14. 2MASS WJ1507476-162738 (L5) (Burgasser 2007): observation (black) and best fitting model (red).

but a little more red, the L3 dwarf J1207 is again slightly cooler. Discrepancies bluewards of 1.5 μm are very small in the fit. Similarly, the water bands and their embossed features agree very well, too. However, the flux in the H and K band peaks is too low in the model. This disagreement is likely a result of the rapidly evolving spectra at this effective temperature range combined with the coarseness of the model grid, because the next cooler model is already too red to produce a good fit.

WJ1506544+132106 (L3; Fig. 13, best fit: $T_{\rm eff}$ = 1700 K, $\log g$ = 4.0, [M/H] = 0.0): Of comparable spectral type and, according to our best fit, comparable effective temperature as J1207, the spectrum of J1506 differs from that of J1207. Our best fit points to a lower surface gravity, which results in an overall higher dust opacity and, thus, in a more red spectrum. The agreement between model and observation is good, especially bluewards of 2 μm.

WJ1507476-162738 (L5; Fig. 14, best fit: $T_{\rm eff}$ = 1800 K, $\log g$ = 5.0, [M/H] = 0.0): J1507 is classified as a mid-L type object (Burgasser 2007). Comparing its NIR spectrum with that of J1506, there is hardly a recognisable feature distinguishing the two. Considering the difference of two subtypes, J1507 is expected to be much cooler than J1506. Instead, our best fits indicate a slightly higher temperature for J1507. Nonetheless, the best fit for J1507 looks quite well. Therefore, it seems reasonable that the difference in the NIR spectral type between J1506 and J1507 might not be as large as their optical classification indicates. The reason for J1507's higher effective temperature is likely the degeneracy of spectra at the given effective temperature regime. This involves that an increased surface gravity is able to compensate most effects of a slightly higher effective temperature. Therefore, two spectra for different model atmosphere parameters look almost alike, as in the case of J1506 and J1507. Employing atmosphere models by Saumon & Marley (2008), Stephens et al. (2009) have found a comparable spectral degeneracy. Hence, their best fit varies between $T_{\rm eff}$ = 1600 K and $\log(g)$ = 4.5 and $T_{\rm eff}$ = 1700 K and $\log(g)$ = 5.5. On the average, this means they have found a slightly lower effective temperature while their surface gravity agrees with our result. The examples of J1507 and J0036, which was also fitted by both Stephens et al. (2009) and us (Table 2), show that the two different atmosphere models agree very well between spectral types L3...L5 and possibly over a wider range.

J1010148-040649 (L6; Fig. 15, best fit: $T_{\rm eff}$ = 1700 K, $\log g$ = 4.5, [M/H] = 0.0): J1010 is noticeably redder in $J - H$ than all previous sample observations. Our best fit to the mid-type L dwarf looks quite good, in general, though the flux in the J band is slightly overestimated while the K band flux is a little too low. The latter points to a lower effective temperature. However, the next cooler model (1600 K) is already significantly too red. A less coarse grid would likely result in a much improved fit of J1010.

J21481628+4003593 & J2244316+204343 (both L6.5pec; Figs. 16, 17, best fits: $T_{\rm eff}$ = 1500 K, $\log g$ = 3.0, [M/H] = −0.3 and $T_{\rm eff}$ = 1500 K, $\log g$ = 3.5, [M/H] = +0.3): Among the most fascinating objects of our sample are J2244 and J2148. Both appear to be closely related and display a dramatically

Table 2. List of additional observations that have not been discussed Sect. 3 but for which we have obtained atmosphere parameters through fitting.

object	Observation			DRIFT-PHOENIX best fit		
designation	optical SpT	NIR SpT	observation by	$T_{\rm eff}$ [K]	log(g)	[M/H]
2MASS J00013044+1010146	–	M6	Burgasser et al. (2004)	2900	4.5	+0.3
2MASS J00583814-1747311	–	M6	Burgasser et al. (2004)	3000	4.5	−0.0
2MASS J01532750+3631482	–	M6	Burgasser et al. (2004)	3000	5.0	−0.0
2MASS J18244344+2937133	–	M6	Burgasser et al. (2004)	3000	4.5	−0.0
LEHPM2-461	M6.5	M7	Burgasser et al. (2008a)	2900	4.5	+0.3
2MASS J15243203+0934386	–	M7	Burgasser et al. (2004)	2800	4.0	−0.0
2MASS J04035944+1520502	–	M7	Burgasser et al. (2004)	3000	5.0	−0.0
2MASS J11323833-1446374	–	M7	Burgasser et al. (2004)	3000	5.0	−0.0
CFHT4	M7	–	Muench et al. (2007)	3000	5.0	−0.0
MHO4	M7	–	Muench et al. (2007)	2900	4.5	−0.0
SO0253+1625	M7	–	Burgasser et al. (2008a)	2900	4.5	+0.3
VB8	M7	–	Burgasser et al. (2008a)	2800	4.0	−0.0
ITG2	M7.25	–	Muench et al. (2007)	2900	5.0	+0.3
2MASS J20491972-1944324	–	M7.5	Burgasser et al. (2004)	2800	4.5	−0.0
2MASS J01470204+2120242	–	M7.5	Burgasser et al. (2004)	2800	4.5	−0.0
KPNO2	M7.5	–	Muench et al. (2007)	2900	4.5	−0.0
KPNO5	M7.5	–	Muench et al. (2007)	2900	4.0	+0.3
CFHT6	M7.5	–	Muench et al. (2007)	2900	3.5	+0.3
2MASS J11150577+2520467	–	M7.5	Burgasser et al. (2004)	2900	5.5	+0.3
CFHT3	M7.75	–	Muench et al. (2007)	2800	4.5	−0.0
2MASS J11150577+2520467	–	M7.5	Burgasser et al. (2004)	2900	5.5	+0.3
2MASS J04414825+2534304	M7.75	–	Muench et al. (2007)	2800	4.5	+0.3
2MASS J23515044-2537367	M8	M8	Burgasser et al. (2008a)	2700	5.0	−0.0
2MASS J00552554+4130184	–	M8	Burgasser et al. (2004)	2700	4.0	−0.0
2MASS J12121714-2253451	–	M8	Burgasser et al. (2004)	2900	4.5	−0.0
2MASS J14171672-0407311	–	M8	Burgasser et al. (2004)	2800	4.5	−0.0
2MASS J17364839+0220426	–	M8	Burgasser et al. (2004)	2800	4.5	−0.0
LRL405	M8	–	Muench et al. (2007)	2700	3.0	−0.0
VB10	M8	M8	Burgasser et al. (2004)	2700	4.5	+0.3
LEHPM1-6443	M8.5	M8	Burgasser et al. (2008a)	2700	4.5	−0.0
2MASS WJ0320284-044636	–	M8.5	Burgasser et al. (2008a)	2500	3.5	−0.3
KPNO9	M8.5	–	Muench et al. (2007)	2600	4.0	−0.0
2MASSJ11240487+3808054	–	M8.5	Burgasser et al. (2004)	2500	5.0	−0.0
LHS2924	M9	–	Burgasser & McElwain (2006)	2500	4.0	−0.0
2MASS J1253+2728	–	M9	Sheppard & Cushing (2009)	2600	5.0	−0.0
KPNO12	M9	–	Muench et al. (2007)	2500	5.0	−0.0
2MASS IJ2107316-030733	–	M9	Burgasser et al. (2004)	2000	5.5	−0.0
DENIS J124514.1-442907	M9.5	M9	Looper et al. (2007)	1900	4.5	−0.0
2MASS PJ0345432+254023	L0	–	Burgasser & McElwain (2006)	1900	5.5	−0.0
2MASS J1230+2827	–	L0	McElwain & Burgasser (2006)	1800	5.0	−0.0
2MASS J12212770+0257198	L0	–	Burgasser et al. (2008a)	1800	5.0	−0.0
2MASS WJ0228110+253738	L0	L0	Burgasser et al. (2008a)	1900	5.5	−0.0
HD89744B	L0	L0	Burgasser et al. (2008a)	1900	5.5	−0.0
2MASS J02271036-1624479	L1	–	Burgasser et al. (2008a)	1800	5.5	−0.0
2MASS WJ0208183+254253	L1	–	Burgasser et al. (2008a)	1800	5.5	−0.0
GJ1048B	L1	L1	Burgasser et al. (2008a)	1800	5.5	−0.0
SDSS J104842.84+011158.5	L1	L4	Burgasser et al. (2008a)	1900	5.5	−0.0
2MASS J15200224-4422419A	–	L1.5	Burgasser et al. (2007)	1900	5.0	+0.3
2MASS WJ1645221-131951	L1.5	–	Burgasser et al. (2008a)	1900	5.0	−0.0
2MASS IJ1807159+501531	L1.5	L1	Burgasser et al. (2008a)	1900	5.5	−0.0
2MASS IJ1807159+501531	L1.5	L1	Burgasser et al. (2008a)	1800	5.5	−0.0
Kelu-1	L2	–	Burgasser (2007)	1800	5.0	−0.0
SSSPM0829-1309	L2	–	Burgasser (2007)	1800	5.5	−0.0
2MASS IJ0847287-153237	L2	L2	McElwain & Burgasser (2006)	1800	5.5	−0.0
2MASS IJ0117474-340325	–	L2	Burgasser et al. (2008a)	1800	4.5	−0.0
2MASS J1431+1436	L2	L2	Sheppard & Cushing (2009)	2100	5.5	−0.0
2MASS J17072343-0558249B	–	L3	McElwain & Burgasser (2006)	1800	5.5	−0.0
2MASS J21512543-2441000	L3	–	Burgasser et al. (2008a)	1600	4.0	−0.0
SDSS pJ224953.45+004404.2	L3	L5	Burgasser et al. (2008a)	1600	4.5	−0.0
SDSS J202820.32+005226.5	–	L3	Burgasser et al. (2008a)	1800	5.5	−0.0
SDSS J232804.58-103845.7	–	L3.5	Chiu et al. (2006)	1800	4.5	+0.3
SDSS J121659.17+300306.3	–	L3.5	Chiu et al. (2006)	1800	5.0	+0.3
2MASS J17111353+2326333	–	L3.5	Chiu et al. (2006)	1800	5.5	−0.0
2MASS J11000965+4957470	L3.5	–	Siegler et al. (2007)	1700	5.0	−0.0
SDSS J134525.57+521634.0	–	L3.5	Chiu et al. (2006)	1800	5.5	−0.0

Table 2. continued.

object designation	Observation optical SpT	NIR SpT	observation by	DRIFT-PHOENIX best fit $T_{\rm eff}$ [K]	log(g)	[M/H]
2MASS WJ0036159+182110	L3.5	L4	Burgasser et al. (2008a)	1800	5.0	−0.0
SDSS J024256.98+212319.6	–	L4	Chiu et al. (2006)	1800	5.0	−0.0
SDSS J153453.33+121949.2	–	L4	Chiu et al. (2006)	1700	4.5	−0.0
SDSS J161731.65+401859.7	–	L4	Chiu et al. (2006)	1600	5.5	+0.3
SDSS J173101.41+531047.9	–	L4	Chiu et al. (2006)	1700	4.5	−0.0
2MASS IJ1104012+195921	–	L4	Burgasser et al. (2004)	1800	5.0	−0.3
2MASS J15200224-4422419B	–	L4.5	Burgasser (2007)	1900	5.5	−0.0
SDSS J083506.16+195304.4	–	L4.5	Chiu et al. (2006)	1700	5.0	−0.0
SDSS J085116.20+181730.0	–	L4.5	Chiu et al. (2006)	1700	5.5	−0.0
SDSS J213240.36+102949.4	–	L4.5	Chiu et al. (2006)	1800	4.5	+0.3
GJ1001B	L5	L4.5	Burgasser (2007)	1700	4.0	−0.0
2MASS J01443536-0716142	L5	–	Burgasser et al. (2008a)	1600	4.0	−0.0
SDSS J154849.02+172235.4	–	L5	Chiu et al. (2006)	1800	5.0	−0.0
SDSS J164916.89+464340.0	–	L5	Chiu et al. (2006)	1800	5.0	−0.0
SDSS J213352.72+101841.0	–	L5	Chiu et al. (2006)	1800	5.0	+0.3
SDSS J020608.97+223559.2	–	L5.5	Chiu et al. (2006)	1800	5.0	−0.0
SDSS J134203.11+134022.2	–	L5.5	Chiu et al. (2006)	1700	5.0	−0.0
2MASS J20025073-0521524	L6	–	Burgasser et al. (2008a)	1600	4.0	−0.0
2MASS IJ0103320+193536	L6	–	Cruz et al. (2004)	1600	3.5	−0.0
2MASS IJ0439010-235308	L6	–	Burgasser (2007)	1800	5.0	+0.3
SDSS J000250.98+245413.8	–	L6	Chiu et al. (2006)	1700	5.0	−0.0
SDSS J065405.63+652805.4	–	L6	Chiu et al. (2006)	1800	5.5	+0.3
SDSS J103321.92+400549.5	–	L6	Chiu et al. (2006)	1800	5.0	−0.0
SDSS J162255.27+115924.1	–	L5	Chiu et al. (2006)	1800	5.0	−0.0
SDSS J163359.23-064056.5	–	L6	Chiu et al. (2006)	1800	4.5	−0.0

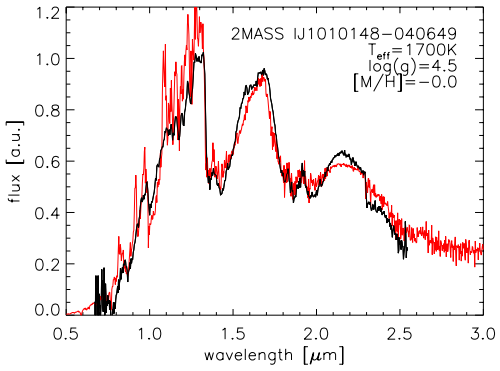

Fig. 15. 2MASS IJ1010148-040649 (L6) (Reid et al. 2006): observation (black) and best fitting model (red).

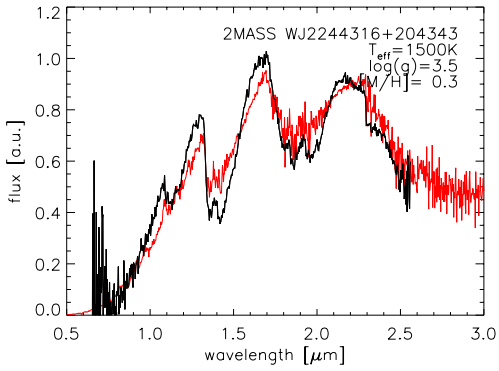

Fig. 17. 2MASS J2244316+204343 (L6.5pec) (Looper et al. 2008): observation (black) and best fitting model (red).

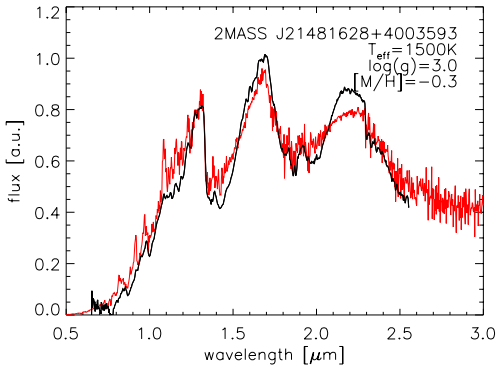

Fig. 16. 2MASS J21481628+4003593 (L6.5pec) (Looper et al. 2008): observation (black) and best fitting model (red).

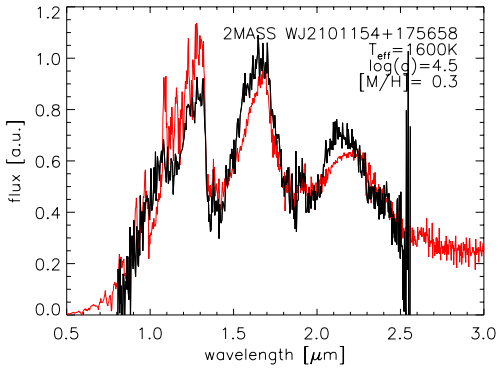

Fig. 18. 2MASS WJ2101154+175658 (L7.5) (Chiu et al. 2006): observation (black) and best fitting model (red).

enhanced H and K flux compared to common L6 types. Looper et al. (2008) reported them to possess an unusually dusty atmosphere, yielding a very red spectrum and weak water bands and weakened alkali lines. According to Looper et al. (2008), unresolved binarity can be excluded as potential reason for the unusual spectra of these objects. Two alternative explanations

for the spectral shape of both objects have been given by Looper et al. (2008), either a low surface gravity or a higher metal abundances. Due to the measured high tangential velocity of J2148, Looper et al. (2008) interpret this object to be old. For this reason they favor the high metallicity scenario within in their conclusions. On the other hand, Looper et al. (2008) agree with McLean et al. (2003) and note the weak KI lines and lacking FeH absorption in the spectrum of J2244, which points to a low gravity. Our models yield the best fitting result for a slight sub-solar metallicity for J2148 and suggest a slight above-solar metal abundance for J2244. The somewhat better fit for J2244 compared to the one for J2148 might be interpreted as an argument for the enhanced metallicity. However, this has to be taken with a grain of salt as both best fits are not extraordinarily well. According to the goodness of fit, the surface gravity appears to be on the low end for both objects. A high gravity scenario seems unlikely, because an increase in gravity eliminates the triangular shape of the H band in the models. Other model parameters than our best fit typically fail to reproduce the water band strength even roughly and retain the JHK colors at the same time. Hence, it appears that the stellar properties are more or less well constrained.

On the other hand, these two extremely red dwarfs belong to the latest type objects that can be fit properly with the present model grid. Unfortunately, the spectra of the next cooler models ($T_{\rm eff}$ = 1400 K) are already much redder than any observed L dwarf. In contrast, the reddening of the models by a decrease in surface gravity is rather small. Hence, there may be a model bias towards lower gravity simply because the reddening by a temperature step is overrated.

Therefore, we remain inconclusive with respect to exact model atmosphere parameters for J2244 and J2148. The noted high tangential velocity of J2148 (Looper et al. 2008) seems to contradict the preference of lower gravity from our best fits, even though low gravity can not be excluded outright. In favor of our models are the weak molecular bands and alkali lines, which are inherently explained by our best fitting models. For the determined model atmosphere parameters of J2244 and J2148, we find dense and optically thick dust clouds. Hence, they strongly blank out the atmospheres below, which are responsible for the bulk of molecular and alkali line opacity as well as the collision induced absorption.

Stephens et al. (2009) have obtained atmosphere parameters of $T_{\rm eff}$ = 1100 K and $\log(g)$ = 5.0 through fitting with Saumon & Marley (2008) models. Their best fitting model matches the near-infrared observational data as good as our does. Also, their model agrees with expectations by Looper et al. (2008) that J2244 possesses an unusually dense dust cloud. However, considering their best fit parameters in Fig. 8 of Saumon & Marley (2008), the respective model suggests a $M_K \sim 14$. Taking into account Fig. 14 of Saumon & Marley (2008), typical objects of this magnitude possess a $J-K \sim 0.5$. The $J-K$ of J2244 differs from this value by almost 2.0. A model of lower magnitude would reduce this discrepancy to about 0.4, because the hybrid sequence has a $J-K \sim 2.1$ for $M_K \sim 13$. Therefore, it seems reasonable that their fit underestimated the effective temperature.

Because the Saumon & Marley (2008) models appear to underestimate the effective temperature of J2244 and our models tend to overestimate it, the real value is likely in between of both best fits.

J2101154+175658 (L7.5; Fig. 18, best fit: $T_{\rm eff}$ = 1600 K, $\log g$ = 4.5, [M/H] = +0.3): J2101 is the latest type object for which we have obtained an acceptable best fit. The three peaks of the observation are not very satisfying. The J band peak is overrated and the shape of the H and K bands is not met. However, the water bands match rather well with respect to band strength and individual features at their bottom.

The best fit parameters point to a too high effective temperature of the object, inconsistent with its given spectral type of L7.5 Chiu et al. (2006). The reason for the mismatch is that J2101 is a binary (Gizis et al. 2003). That appears to have a significant influence on the individual components, which is why neither a single model nor a simple superposition of two models (not shown) is able to fit the object satisfyingly well. In the latter case, either the near-infrared colors are not matched or the molecule bands strength is underestimated. Therefore, we assume that irradiation and other binarity effects would need to be considered in order to improve the fit.

4. General discussion

The previous section focused on individual objects. This section is aimed at investigating systematic limits of the model. For this, all 108 selected observations have been fit. The best fitting parameters for the 90 objects which have not been discussed in the previous section are listed in Table 2. All 108 objects are shown in effective temperature-spectral type diagrams (Fig. 20).

Even though there appear to remain many discrepancies between the Drift-Phoenix model and observations, it reproduces the M-L transition quite well. Especially, since it does not rely on free parameters that tune the amount of dust. Golimowski et al. (2004) have established an empirical effective temperature-spectral type relation. A refined version of this has been released by Stephens et al. (2009). Their polynomial fits to their data are shown in Fig. 20. Though the agreement between our models and empirical results is not yet completely satisfying, the general trend is already well matched. The effective temperatures are likely underestimated by our models around spectral type L0. For later spectral types, they are mildly overestimated. The sytematic disagreement between our models and the Stephens et al. polynomes for the mid-M dwarfs is possibly due to the comparably low number of data points that contributed to the polynome fitting at this range.

The employed broadband fitting represents a challenging performance test for model grids, because all the various spectral features need to match at once in order to find an acceptable fit. Therefore, deviations between models and observations are much more pronounced than for a fitting of narrow spectral bands.

As Figs. 1–18 prove, the Drift-Phoenix models are able to obtain reasonable fits for most of the given near-infrared data and provide a self-consistent impression for the M-L transition region. Despite that, there is still much need for improvement.

For instance, the models exhibit a too small dust opacities above $T_{\rm eff}$ = 1900 K (Fig. 19). The symptom of this is the gap in the best fitting effective temperatures for the M9...L1 types (Fig. 20). Most fits for M9 observations indicate an effective temperature of roughly 2500 K. Over the following 2 subtypes (L0, L1), the best fitting models indicate about $T_{\rm eff}$ = 1900 K. As a side effect, the goodness-of-fit is worsening notably in these models. The largest mismatch occurs for the M9/L0 types and vanished completely before the L3 type. The apparent reason is a too low dust opacity in the present models for $T_{\rm eff} \geq 1900$ K. Since there appears to be less dust opacity than there should be, the involved model spectra are slightly bluer. Other atmosphere models face similar effects around the M/L transition

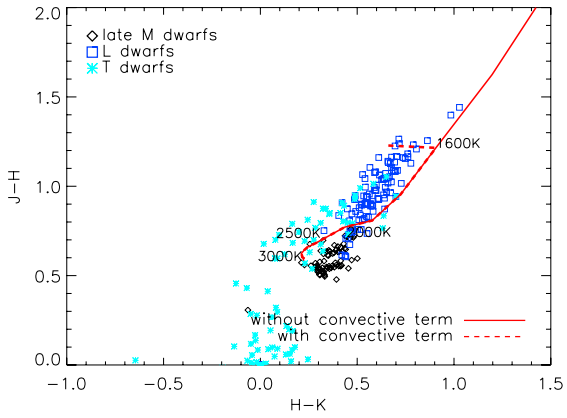

Fig. 19. Color diagram for the 2MASS *JHK* filters. Late M dwarf (*black diamonds*), L dwarf (*blue rectangles*) and T dwarf (*blue stars*) observations are indicated. The red curve corresponds to a log(g) = 5.0 and solar abundance model sequence of the current Drift-Phoenix grid. The dotted line indicate the model color trend, if detached convection zones are considered in the grain motion.

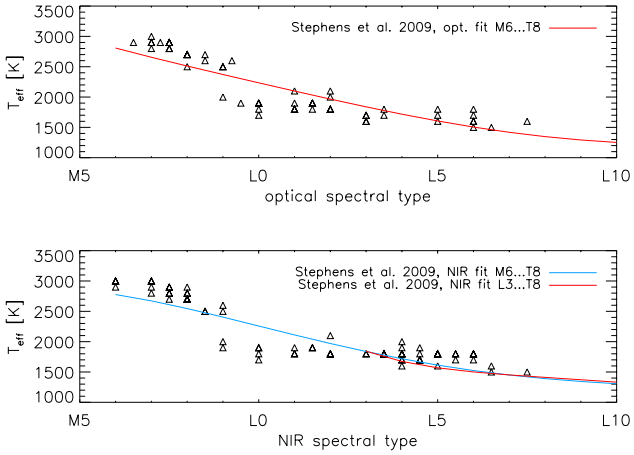

Fig. 20. Relation between the given optical spectral types of 57 objects and respective Drift-Phoenix best fitting effective temperatures is shown in the *upper panel*. The *lower panel* depicts a similar relation for NIR spectral types of 75 objects. Both panels feature empirical fits by Stephens et al. (2009) for comparison.

(e.g., Saumon & Marley 2008, Fig. 10), which points out clearly that the physics of involved atmospheres is still not fully understood.

With respect to fitting observation, a slightly lower effective temperature is partially able to compensate for the bluer models. However, such an alleged shift in the effective temperature will be accompanied by systematic errors in spectral features, i.e., it results in a worsened goodness-of-fit for the involved spectral subtype. Therefore, fits for the L0 types as well as some M9 types provide best fit effective temperatures that are systematically ∼400 K too cool, compared to the expected flat relation and also empirical relations shown in Fig. 20. For the L1 and L2 types the effective temperatures are underestimated by up to 250 K. Note that such deviations are especially pronounced for the broadband low resolution fitting which we have applied for this work. A narrow band high resolution fitting will likely result in a less pronounced deviation.

The reason for the lacking dust opacity might either be due to a too conservative approximation of the element replenishment or other relevant reaction paths for condensation which have not been considered yet. The exact details are presently under investigation.

A completely different problem of the model grid is the overestimated dust opacity for $T_{\rm eff} \leq 1600$ K. In the models, the dust opacity increases exponentially for decreasing effective temperatures. This is not surprising as a lower temperature yields a higher supersaturation of the gas and, thereby, results in larger amounts of dust. Below $T_{\rm eff} = 1800$ K, dust opacity has become so huge that even small steps in the model atmosphere parameters can result in very different spectra. Hence, a higher resolution of the model grid, with respect to the atmosphere parameters, might become necessary in order to obtain more precise model atmosphere parameter estimates through fitting and to avoid ambiguities at the given effective temperature range. More challenging, however, is another aspect of the growing dust opacity of the models. While the model spectra become more and more red in the NIR (Fig. 19), observed spectra later than type L5 reach a certain redness and consecutively turn blue again. In other word, there exists another self regulation mechanism in real objects that destroys the dust cloud below a given effective temperature.

Until such a mechanism is introduced into the dust model, the Drift-Phoenix models remain unable to obtain satisfying fits for cooler effective temperatures than 1500 K. Below, the mentioned overly red model spectra raise the goodness-of-fit enough to prohibit best fits for lower effective temperatures. Hence, a jamming around $T_{\rm eff} = 1600$ K is noticable for later spectral types than L4 (Fig. 20).

In order to overcome the problem of overestimated dust opacity, the hybrid model sequence by Saumon & Marley (2008) is undergoing a steep rise of their sedimentation parameter at the respective effective temperature range. This results in an almost instant destruction of the dust cloud. Due to this, their sequence reproduces colors and magnitudes around the L/T transition very successfully. A necessary step is now to get rid of parametrisations and to find an explanation for this rapid loss of dust opacity.

A potential explanation might be the formation of detached convection zones (Burgasser et al. 2002; Burrows et al. 2006) at the bottom of the dust clouds, which is a direct result of the cloud's backwarming. According to our models, such zones begin to form below $T_{\rm eff} = 1700$ K. The resulting convective velocities are considerably higher than the fall velocities of typical dust grains at the respective atmospheric layers. Therefore the gas flows will dominate the grain motion. This means convection might act like a fan that blows a significant portion of the lower cloud grains into hotter atmosphere regions and accelerate their evaporation. For this reason, we have tested a convective motion term into the fundamental dust moment equations of our model. Indeed, this breaks the false reddening of models below $T_{\rm eff} = 1700$ K (dotted line in Fig. 19). The model colors begin to turn blue again, just as it is observed in real objects. There is, however, a limit to this improved approach. A proper model convergence is only achieved between $T_{\rm eff} = 1500...1600$ K. For cooler models, numerical oscillations of atmosphere properties turn up. A timescale argument is able to illustrate what this implies: for the given effective temperature range, dust grains will take between months and decades to cross the lower cloud layers, depending on the atmosphere parameters. Assuming that these layers begin with a depleted gas phase and no dust, it will take a comparable amount of time before a sufficiently dense cloud has accumulated. Only then, convection will set in and result in the destruction of much of the locally present dust. As soon as the dust opacity has dropped sufficiently, convection will end and the cycle will start anew. Therefore, it appears

that there is a local variability of the dust cloud on the time scale of months. However, we must note that local variability phases, statistically mapped on a stellar surface, must not result in a global and directly observable variability. Most likely, the total observed flux will remain nearly static. Nonetheless, strong statistical variations in this mapping can result in multitude of different spectra for exactly the same atmosphere parameters. This might turn out as possible, if painful, explanation for the observation of extraordinary blue and red L dwarfs. Such observations, as for instance J2244 and J2148 by Looper et al. (2008), exhibit either too dense or too rare dust clouds. Typically, explanations relegate to unusual surface gravities or metallicities. However, such extreme parameters must not necessarily be required if the dust opacity distributed chaotically.

A third point is that, for the higher effective temperatures, the employed low resolution wide band fitting is not very sensitive to the comparably weak gravity-dependent features. Only for models with a notable dust opacity, the determined gravity becomes more reliable as a distinguishable goodness-of-fit arises between different $\log(g)$ models. Hence, there is no way around high resolution comparisons of smaller bands if one is interested in inferring a precise surface gravity. In other words, this is an issue of the fitting method and not the models itself. In a few rare cases, degenerate spectra at lower temperatures combined with the low resolution fitting can account for up to one dex of $\log(g)$ uncertainties.

Other uncertainties arise due to the model grid coarseness, the model systematics and observational noise.

5. Comparison with earlier Phoenix models

The Cond/Dusty-Phoenix models (Allard et al. 2001) have been widely used for years and helped to understand the two limiting cases of brown dwarf atmospheres that are either covered by thick cloud layers (Dusty) and those where the cloud is located beneath optically thick gaseous atmosphere (Cond). Both assume a phase equilibrium between gas and dust. While the Dusty approach fully considered the opacity of the calculated amount of dust, it was neglected for the Cond case where the dust was assumed to have settled completely. Hence, the Dusty models are not too far astray for the warmer late M dwarfs. In contrast to that, the Cond models strongly underestimate the influence of dust throughout the L dwarf regime, thus, yielding fair results only for cooler objects. The most prominent example for the application of the Dusty/Cond models are brown dwarf evolutionary models in order to find the relation between evolution and spectral appearance. Figure 1 of Chabrier et al. (2000) demonstrates the uncertainty for the evolutionary tracks due to different boundary conditions provided by Dusty- and Cond-Phoenix model atmospheres. Recently, Mohanty et al. (2010) have used the Dusty/Cond-Phoenix models to determine the primary's effective temperature of the eclipsing binary 2MASS J05352184-0546085. They have made use of high resolution spectra of the TiO-ϵ band and the KI doublet separately and have inferred $T_{\rm eff}$ to a precision ±50 K.

Figure 21 compares models for each of the three approaches, Dusty, Cond and Drift, for the same model atmosphere parameters we have obtained for 2MASS J1010 ($T_{\rm eff}$ = 1700 K, $\log(g)$ = 4.5, [M/H] = 0.0). As Fig. 15 demonstrates, the Drift-Phoenix model fits the observation quite nicely. The older models differ considerably from the Drift model. As one might expect they are either much bluer or redder. Especially for the Cond spectrum the water band strength is way overestimated. The good fit of the new models with the observation over the whole considered spectral range can not be matched by any Cond or Dusty spectra. The two respective best fits with the given best fitting model of Drift are shown in Fig. 21. Both do not reproduce the near infrared colors or water band strength of either the observation or the Drift model spectrum. Also, the TiO bands (e.g., ϵ band: ~0.843 . . . 0.846 μm) vary considerably between synthetic spectra of the three model approaches. The stellar parameters determined by these best fits differ strongly. Especially the Dusty model fit is hotter than both other models because it overestimates the amount of dust. However, it roughly agrees with our surface gravity estimate with Drift. In contrast, Cond models are not at all able to yield a comparable water band strength for these low gravities.

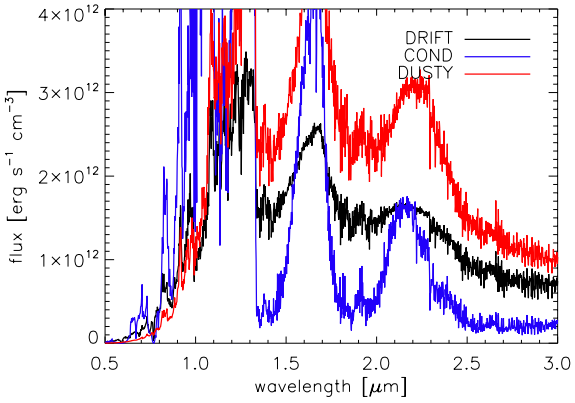

Fig. 21. Comparison between Cond-, Dusty- and Drift-Phoenix models for a given set of model atmosphere parameters. All three models are shown for the Drift-Phoenix best fit parameters of 2MASS J1010 ($T_{\rm eff}$ = 1700 K, $\log(g)$ = 4.5, [M/H] = 0.0).

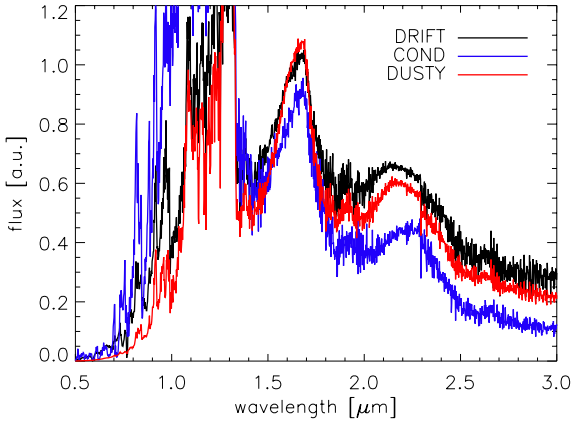

Fig. 22. Comparison of best fitting synthetic spectra for 2MASS J2002 for the three different atmosphere models: Cond- ($T_{\rm eff}$ = 2400 K, $\log(g)$ = 3.0, [M/H] = 0.0), Dusty- ($T_{\rm eff}$ = 1800 K, $\log(g)$ = 5.5, [M/H] = 0.0) and Drift-Phoenix ($T_{\rm eff}$ = 1700 K, $\log(g)$ = 4.5, [M/H] = 0.0).

6. Summary

We conclude that the Drift-Phoenix models reproduce observations well over much of the considered range of atmosphere parameters. In summary, the present model grid is able to provide good fitting results for spectral types M6 to L6.

Above $T_{\rm eff}$ = 1900 K, the model underestimates the dust opacity slightly, which is most likely a result of an underestimated mixing efficiency of the atmosphere. Therefore, the involved models typically feature too blue NIR spectra, which

results in an underestimation of the effective temperature for the wide band fitting method employed in this work.

Presently, spectral types later than L6 can not be reproduced properly because cooler models possess too strong dust opacities. This problem can be attributed to a currently unidentified self regulation mechanism of the dust cloud. Without such a mechanism, NIR colors of late L type observations would not be turning bluer. At the moment, this dust opacity problem can only be treated by manually adjusting the amount of dust, as done by other modeler groups. The gain from such an approach remains unsatisfying. The substellar atmosphere dust modeling community is still lacking the means to explain this sudden drop of dust opacity which is one of the key processes at the L-T transition.

The Drift-Phoenix models begin to develop detached convection zones within their inner dust cloud at about the same effective temperature where there seems to be an overestimated dust opacity.This suggests a correlation between turbulent motion of the atmosphere and the amount dust. A modified approach, considering these detached convection zones in the grain motion, has proven to stop the immense reddening trend of the NIR colors at about the correct effective temperature. However, it turned out that the cycle of dust accumulation, convection and dust evaporation can not be solved time-independent for cooler models due to exceedingly growing oscillations between iterations. We conclude that statistical mapping of time-dependent states of the cloud onto a stellar surface will no longer provide unambiguous spectra. This implies that objects of similar atmosphere parameters may come with a wide variety of spectra. Such may provide an explanation for unusually red and blue L dwarfs which does not rely on extreme constellations of the surface gravity and metallicity. Instead, there might be an additional statistical degree of freedom aside from the stellar parameters that is determining the spectral appearance of mid/late L dwarfs.

Acknowledgements. Some of the calculations presented here were performed at the Höchstleistungs Rechenzentrum Nord (HLRN); at the Hamburger Sternwarte Apple G5 and Delta Opteron clusters financially supported by the DFG and the State of Hamburg; and at the National Energy Research Supercomputer Center (NERSC), which is supported by the Office of Science of the US Department of Energy under Contract No. DE-AC03-76SF00098. We thank all these institutions for a generous allocation of computer time. This research has benefited from the M, L and T dwarf compendium housed at DwarfArchives.org and maintained by Chris Gelino, Davy Kirkpatrick and Adam Burgasser. S.W. thanks the Research Training Group 1351 of the German Research Foundation for funding. Furthermore, S.W. acknowledges the hospitality of St. Andrews University where parts of this paper was written. Also, C.H. acknowledges the hospitality of Kavli Institute for Theoretical Physics (University of California). This research was supported in part by the National Science Foundation under Grant No. NSF PHY05-551164.

References

Ackerman, A. S., & Marley, M. S. 2001, ApJ, 556, 872
Allard, F., Hauschildt, P. H., Alexander, D. R., & Starrfield, S. 1997, ARA&A, 35, 137
Allard, F., Hauschildt, P. H., Alexander, D. R., Tamanai, A., & Schweitzer, A. 2001, ApJ, 556, 357
Baron, E., Hauschildt, P. H., Allard, F., et al. 2003, in Modelling of Stellar Atmospheres, IAU Symp., 210, 19
Becklin, E. E., & Zuckerman, B. 1988, Nature, 336, 656
Bruggeman, D. A. G. 1935, Ann. Phys., 24, 636
Burgasser, A. J. 2007, ApJ, 659, 655
Burgasser, A. J., & McElwain, M. W. 2006, AJ, 131, 1007
Burgasser, A. J., Marley, M. S., Ackerman, A. S., et al. 2002, ApJ, 571, L151
Burgasser, A. J., McElwain, M. W., Kirkpatrick, J. D., et al. 2004, AJ, 127, 2856
Burgasser, A. J., Looper, D. L., Kirkpatrick, J. D., & Liu, M. C. 2007, ApJ, 658, 557
Burgasser, A. J., Liu, M. C., Ireland, M. J., Cruz, K. L., & Dupuy, T. J. 2008a, ApJ, 681, 579
Burgasser, A. J., Looper, D. L., Kirkpatrick, J. D., Cruz, K. L., & Swift, B. J. 2008b, ApJ, 674, 451
Burgasser, A. J., Witte, S., Helling, C., & Hauschildt, P. H. 2009, ApJ, 697, 148
Burrows, A., & Sharp, C. M. 1999, ApJ, 512, 843
Burrows, A., Sudarsky, D., & Hubeny, I. 2006, ApJ, 640, 1063
Chabrier, G., & Baraffe, I. 2000, ARA&A, 38, 337
Chabrier, G., Baraffe, I., Allard, F., & Hauschildt, P. 2000, ApJ, 542, 464
Chiu, K., Fan, X., Leggett, S. K., et al. 2006, AJ, 131, 2722
Cooper, C. S., Sudarsky, D., Milsom, J. A., Lunine, J. I., & Burrows, A. 2003, ApJ, 586, 1320
Cruz, K. L., Burgasser, A. J., Reid, I. N., & Liebert, J. 2004, ApJ, 604, L61
Dehn, M. 2007, Ph.D. Thesis, Universität Hamburg
Gail, H.-P., Keller, R., & Sedlmayr, E. 1984, A&A, 133, 320
Gizis, J. E., Reid, I. N., Knapp, G. R., et al. 2003, AJ, 125, 3302
Golimowski, D. A., Leggett, S. K., Marley, M. S., et al. 2004, AJ, 127, 3516
Hauschildt, P. H., & Baron, E. 1999, J. Comp. Appl. Math., 109, 41
Hayashi, C. 1962, Pub. A.S.J., 13, 450
Helling, C., & Woitke, P. 2006, A&A, 455, 325
Helling, C., Ackerman, A., Allard, F., et al. 2008a, MNRAS, 391, 1854
Helling, C., Dehn, M., Woitke, P., & Hauschildt, P. H. 2008b, ApJ, 675, L105
Helling, C., Woitke, P., & Thi, W.-F. 2008c, A&A, 485, 547
Jones, H. R. A., & Tsuji, T. 1997, ApJ, 480, L39
Kirkpatrick, J. D. 2005, ARA&A, 43, 195
Kirkpatrick, J. D., Barman, T. S., Burgasser, A. J., et al. 2006, ApJ, 639, 1120
Kleinmann, S. G. 1992, in Robotic Telescopes in the 1990s, ed. A. V. Filippenko, ASP Conf. Ser., 34, 203
Kraus, A. L., & Hillenbrand, L. A. 2009, ApJ, 704, 531
Kumar, S. S. 1963, ApJ, 137, 1126
Looper, D. L., Burgasser, A. J., Kirkpatrick, J. D., & Swift, B. J. 2007, ApJ, 669, L97
Looper, D. L., Kirkpatrick, J. D., Cutri, R. M., et al. 2008, ApJ, 686, 528
Ludwig, H.-G., Allard, F., & Hauschildt, P. H. 2002, A&A, 395, 99
Lunine, J. I., Hubbard, W. B., & Marley, M. 1986, ApJ, 310, 238
McElwain, M. W., & Burgasser, A. J. 2006, AJ, 132, 2074
McLean, I. S., McGovern, M. R., Burgasser, A. J., et al. 2003, ApJ, 596, 561
Mie, G. 1908, Annalen der Physik, 25, 377
Mohanty, S., Stassun, K. G., & Doppmann, G. W. 2010, ApJ, 722, 1138
Muench, A. A., Lada, C. J., Luhman, K. L., Muzerolle, J., & Young, E. 2007, AJ, 134, 411
Nakajima, T., Oppenheimer, B. R., Kulkarni, S. R., et al. 1995, Nature, 378, 463
Neuhäuser, R., Schmidt, T. O. B., Seifahrt, A., et al. 2009, in Cool Stars 15 Proceedings, 15th Cambridge Workshop
Noll, K. S., Geballe, T. R., & Marley, M. S. 1997, ApJ, 489, L87
Rebolo, R., Zapatero-Osorio, M. R., & Martin, E. L. 1995, Nature, 377, 129
Reid, I. N., Lewitus, E., Burgasser, A. J., & Cruz, K. L. 2006, ApJ, 639, 1114
Reid, I. N., Cruz, K. L., Kirkpatrick, J. D., et al. 2008, AJ, 136, 1290
Ribas, I. 2003, A&A, 400, 297
Rice, E. L., Barman, T., McLean, I. S., Prato, L., & Kirkpatrick, J. D. 2010, ApJS, 186, 63
Saumon, D., & Marley, M. S. 2008, ApJ, 689, 1327
Schmidt, T. O. B., Neuhäuser, R., Seifahrt, A., et al. 2008, A&A, 491, 311
Sheppard, S. S., & Cushing, M. C. 2009, AJ, 137, 304
Siegler, N., Close, L. M., Burgasser, A. J., et al. 2007, AJ, 133, 2320
Stephens, D. C., Leggett, S. K., Cushing, M. C., et al. 2009, ApJ, 702, 154
Tinney, C. G. 1998, MNRAS, 296, L42
Tsuji, T., Ohnaka, K., Aoki, W., & Nakajima, T. 1996, A&A, 308, L29
Whitworth, A. P. 2007, in IAU Symp., ed. B. G. Elmegreen, & J. Palous, 237, 251
Witte, S., Helling, C., & Hauschildt, P. H. 2009, A&A, 506, 1367
Woitke, P., & Helling, C. 2003, A&A, 399, 297
Woitke, P., & Helling, C. 2004, A&A, 414, 335
Wolf, S., & Voshchinnikov, N. V. 2004, Comp. Phys. Commun., 162, 113